Design of Composite Tidal Turbine Blades

David M. Grogan, Sean B. Leen, Ciaran R. Kennedy, Conchúr M. Ó Brádaigh,
Mechanical and Biomedical Engineering, NUI Galway, Ireland

Abstract

Tidal turbine blades are subjected to significant thrust and torsional loadings due to the high density of the seawater in which they operate. These thrust loadings lead to high bending moments at the blade root, which can prove to be a serious design constraint for these devices and can have implications with respect to cost-effectiveness and scalability. This work presents a combined hydrodynamic-structural design methodology for a commercial scale (1.5 MW) tidal turbine. A hydrodynamic analysis of the blade is carried out to determine force distributions along the blade span under normal and extreme operating conditions. Using output from the hydrodynamic model, a pre-processor for computing blade structural properties is used to determine the strain distribution along the blade spar caps. The strain distributions from this analysis are then compared with a finite element model of the blade which is then used to compare the structural performance of glass fibre reinforced polymer (GFRP) and carbon fibre reinforced polymer (CFRP) as spar cap materials.

Keywords: Tidal turbine blades; Structural design; Hydrodynamics; Composites; Glass fibre; Carbon fibre

[1]

1. Introduction

The evolution and improvement of sustainable energy systems is of growing importance. While the development of technologies related to the exploitation of natural wind resources continues apace, the potential of a long neglected renewable energy source, ocean energy, is

[1] **Abbreviations**

GFRP	Glass fibre reinforced polymer
CFRP	Carbon fibre reinforced polymer
BEMT	Blade element momentum theory
PreComp	Pre-Processor for computing composite blade properties
UD	Unidirectional
DB	Double-bias
FEA	Finite element analysis

finally being realised. If this energy can be successfully harnessed, it presents the opportunity to ensure greater security of energy supply, significantly reduce greenhouse gas emissions, and allow some countries to possibly become net exporters of energy, which would naturally have positive economic implications.

One of the main benefits of tidal energy over other renewables such as solar and wind energy is that energy production is predictable over long time scales due to the well documented behaviour of the tides [1]. Additionally, the power output from a typical horizontal axis tidal turbine is significantly greater than for a wind turbine of similar dimensions and comparable fluid flow velocities, due to water being over 800 times denser than air [2]. In spite of these inherent advantages, tidal current turbine technology is still in its infancy, with the world's first large scale commercial tidal turbine only having been connected to the grid as recently as 2008 by Sea Generation Ltd [3].

The majority of tidal energy devices developed to date use a rotating horizontal axis turbine as their basis [3]. The principle of operation of this class of turbines is similar to horizontal axis wind turbines [4]. The blades of the turbine create lift due to the resultant hydrodynamic forces of the inflow which is perpendicular to the rotor plane. These forces cause the blades to rotate and the resulting torque is transferred via a shaft and gearbox to a generator. Higher solidity-ratio designs are sometimes favoured over lower ratio designs as they generate greater starting torque and reduce balancing issues. A downside to using more blades is that hydrodynamic losses are increased [3]. Blade pitching is also used extensively to limit peak power so that generator capacity is not exceeded. Horizontal axis tidal turbines encounter problems which do not affect wind turbines, such as cavitation at the blade tips [5] and also experience relatively higher blade root bending moments due to the higher density of water.

Composite materials are the material of choice for large wind turbine blades; with glass fibre reinforced polymer (GFRP) and carbon fibre reinforced polymer (CFRP) being most commonly used [6]. The high specific strength and stiffness offered by such materials, as well as their apparent resistance to corrosion in a sub-sea environment, makes them an attractive choice for use in tidal turbine blades. GFRP materials, due to their good structural properties and low cost, are generally seen as the first port of call for blade designers who are seeking to produce a cost effective design. High performance CFRP offer improved performance over GFRP, but at a higher cost. While all but the largest wind turbine blades

can be constructed primarily from GFRP due to the relatively low loadings in question, the high density of sea-water means that even modest sized tidal turbines will be subjected to significant working loads.

One challenge for blade designers is to determine the stage at which the use of high performance CFRP becomes economically justifiable. This paper seeks to develop a design methodology for tidal turbine blades based on a combined hydrodynamic-structural model with a view to exploring the suitability of using GFRP and CFRP as blade construction materials. Blade Element Momentum Theory (BEMT), which is a method for analysing the aerodynamic or hydrodynamic performance of wind or tidal turbines, is employed in the hydrodynamic design of the blade. BEMT is an established approach based on a modified version of Glauert propeller theory [7] and is itself a combination of two separate theories, namely one-dimensional momentum theory with rotational momentum, and blade element theory. Using a stream-tube model based on BEMT, it is possible to calculate steady loads on the turbine blades which in turn can be used to calculate the thrust and power of the rotor for varying fluid velocities, rotational speeds and pitch angles, as well as being used to define optimised chord and pitch angle distributions along the span of the blade for a given set of input parameters [8].

With the stream-tube model producing sufficient information about the dimensions and forces acting on the turbine blades it is possible to proceed with the structural design of the blade using a programme called PreComp (Pre-Processor for computing composite blade properties) which is a code developed by *The National Wind Technology Center* [9]. Using output from the stream-tube model, PreComp facilitates the calculation of key structural properties such as: flap-wise and edge-wise section stiffness, the mass of the blade per unit length and the section torsional stiffness amongst others. Hence, it is possible to calculate material strain distributions along a blade for a range of materials, load scenarios and composite lay-up configurations.

In the present work, the preliminary strain distributions calculated using the combined hydrodynamic-structural model based on PreComp, are compared with those obtained from a more detailed and realistic finite element model of a full-scale tidal turbine blade. The structural performance of GFRP and CFRP commercial scale tidal turbine blades under

typical operating conditions are then evaluated using both methodologies, i.e. using PreComp and 3D models of the blades under hydrodynamic loads.

2. Methodology

The blade design approach outlined consists of a combined hydrodynamic-structural model. The hydrodynamic model requires a number of fundamental parameters to be defined including the tidal stream velocity and several key dimensions of the blade which will dictate the power output of the turbine. The axial and tangential forces acting on the blade as well as the optimal chord length and pitch angle distributions for the blade are provided by the hydrodynamic model and are used as inputs for the structural model, which is based on a pre-processor for computing structural properties and a finite element model of the blade. The structural model provides the strain distribution along the span of the blade and hence the maximum strain present which can be used as a criterion for material selection.

2.1 Hydrodynamic Model

2.1.1 Stream-tube Model

In modelling a tidal turbine it is assumed that only the mass of fluid which passes through the rotor disc area slows down and loses some of its kinetic energy. This assumption facilitates the definition of a boundary surface which separates the affected mass of water from the non-affected water and can be extended upstream and downstream from the rotor to form a stream-tube of circular cross-section. This stream-tube can be divided into a number of individual concentric stream-tubes with each stream-tube corresponding to an annular area of the rotor disk. Thus each individual blade is divided into a number of elements at a radius r and of length δr along its span. The chord length of each of these blade elements can be adjusted until the fluid forces acting on it are balanced by the momentum thrust of the flow field as outlined by BEMT. The process is carried out for each blade element along the span of the blade, with the total thrust acting on the blade being found by summing the elemental thrusts. The total torque, and hence the power, is calculated by multiplying the tangential force on each blade element by the span wise distance of the element from the blade root and then summing the result from each blade element.

BEMT is based on the premise that the thrust and torque forces can be derived through the use of two-dimensional hydrofoil characteristics, using an angle of attack calculated from the incident resultant velocity in the cross-sectional plane of the blade element. The angle of attack, α, is determined by the components of velocity at a radial position on the blade expressed as a function of the tidal current speed, the flow factors (describing the decrease in tidal stream velocity between the free stream and the rotor plane) as well at the rotational speed of the turbine blade as shown in Fig. 1. With information about how the lift coefficient and the drag coefficient vary with the angle of attack of the hydrofoil, the forces on the blade for known axial and tangential flow induction factors can be determined. The hydrodynamic model used here is based on the work of *Kennedy et al* [10].

The analysis proceeds by defining a tidal turbine with N blades, each of which having an end tip radius of r and a span-wise varying chord length of c. The angle between the zero lift line of the aerofoil and the plane of the disc can also vary in a span-wise direction and is denoted by the pitch angle β. The velocity at the rotor disk, U_d, is given by

$$U_d = U_\infty(1-a) \tag{1}$$

where U_∞ is the free-stream velocity and a is the axial flow induction factor. The tangential velocity of a blade element, v_b, is given by

$$v_b = \omega r \tag{2}$$

where ω is the angular velocity of the blade. When this velocity component is combined with the expression for the tangential velocity of the wake the result is the net tangential flow velocity experienced by a blade element, v_t, which is

$$v_t = (1+a')\omega r \tag{3}$$

where a' is the tangential flow induction factor. The overall resultant relative velocity that the blade experiences, W, is therefore

$$W = \sqrt{U_d^2 + {v_t}^2} \tag{4}$$

This resultant velocity is seen to act at an angle φ to the plane of rotation of the blade, which is given by

$$\varphi = \alpha + \beta \tag{5}$$

The lift and drag forces for each span-wise blade element can be derived from Fig 1. The lift force acts normal to the direction of W and its magnitude at each span-wise location, δL, can be calculated using the following equation

$$\delta L = \frac{1}{2}\rho W^2 c C_L \delta r \tag{6}$$

Similarly, the drag force, which acts parallel to the resultant relative velocity, is given by

$$\delta D = \frac{1}{2}\rho W^2 c C_D r \delta r \tag{7}$$

Where δD is the drag force at each span-wise location and C_L and C_D are the lift and drag coefficients respectively.

With knowledge of the hydrodynamic forces acting on a given blade element, it is possible to resolve these forces into their axial and tangential components. The axial force component, F_A, acting on a blade element is

$$F_A = \delta L \cos\varphi + \delta D \sin\varphi \tag{8}$$

While the tangential force component, F_t, is given as

$$F_t = \delta L \sin\varphi + \delta D \cos\varphi \tag{9}$$

As mentioned previously, with knowledge of the axial and tangential forces acting on each blade element it is possible to calculate the total thrust force acting on a blade as well as the total torque developed. It should be noted that BEMT has a number of limitations. Due to each blade element being treated as a 2D segment in terms of the forces acting on it, spanwise

flow is neglected which could introduce errors for rotors with significant pressure gradients along the blade length. Another issue is that large out of plane deflections of the blade can lead to deviations from the fundamental BEMT. In this study, blade deflections are within an acceptable range for BEMT to still apply without introducing significant error.

2.1.2 Hydrodynamic Design Process

A flowchart of the hydrodynamic design process in shown in Fig. 2. This is described by the following algorithm:

Step 1 - Initial design specifications

The main design constraints include the desired rated power of the turbine, the number of blades on the rotor and the operating flow velocity. In this case, the rated power output of the turbine was chosen to be 1.5 MW, with a three-bladed rotor configuration. This is in keeping with the typical power output of current wind turbines and with what was deemed to be a commercially viable design. The normal and extreme flow velocities under which this turbine was expected to operate were chosen as 2.4 ms^{-1} and 4.1ms^{-1} respectively, and represent the two main load scenarios for the turbine blades. These flow velocity selections were based on data from possible tidal turbine farm sites [10] [11]. Note that the tidal current velocity and number of turbine blades are entered as inputs to the stream-tube model, with the rated power being an output.

Step 2 - Hydrofoil selection

With these initial turbine specifications decided upon, an appropriate hydrofoil for the blade is selected based on lift and drag coefficients, which, as mentioned previously, directly affect the power output of the turbine and are used as inputs for the stream-tube model. In addition, the hydrofoil must have a suitable thickness near the blade root to resist the anticipated high bending moments. It must also be insensitive to surface roughness effects for the expected pressure ratios during normal operation. A high coefficient of lift at high angles of incidence is important due to the circular plane in which the blade operates [8]. However, having a range of high lift coefficients also leaves the blade susceptible to stall and flow separation, which are detrimental to efficiency and cause power losses [8] [12]. To this end, the Riso A1

family of aerofoils [13, 14] are chosen here as they offer high lift-to-drag ratios over a wide angle of attack range, coupled with a relatively thick cross section to improve structural properties. The lift-to-drag ratio, lift coefficient and angle of attack from the Riso aerofoil are used as inputs to the stream-tube model.

Other inputs affecting the rated power are the rotor size and rotational speed of the turbine. Unlike the inputs relating to the Riso aerofoil, the dimensions of the rotor and its rate of rotation cannot be determined directly. Hence an iterative method is required to arrive at an appropriate design (see below). With arbitrary values for these inputs included, the stream-tube program outputs the rated power, the axial and tangential forces acting on the blade and the optimal chord length and pitch angle distributions for the blade for the given turbine configuration. If the predicted rated power does not match the project specifications, then changes must be made to the hydrofoil selection or rotor size. Given the well documented and favourable performance of the Riso aerofoil for this application, the design iteration is focused on varying the rotor size in order to achieve the desired power output. It should be noted that the rotor dimensions and rate of rotation also affect the efficiency of the turbine for a given flow velocity, which is output by the stream-tube model.

Step 3 - Turbine rotor sizing

The main constraint imposed on rotor size is the water depth in which tidal energy devices can be installed [15]. The depth at which tidal turbines can operate is limited by the proximity of the blade tips to the free-surface due to the effects of wave loading which become problematic near the water surface [16]. The depth of operation is also constrained by the depth to which the support structure can be successfully installed, which is approximately 40 m to 50 m for the current generation of tidal turbines [15]. A report released by the European Commission [17] suggests that a full scale tidal turbine should occupy approximately half the depth of the channel where it is to be installed. Combining this recommendation with the maximum depth at which current support structures can be constructed limits the rotor to a maximum diameter of approximately 25 m. In addition, excessively long blades can generate prohibitively large bending moments at the root of the blade [10], meaning a shorter blade would be preferable.

Step 4 – Turbine rate of rotation optimisation

The effect of rotational speed on rated power and efficiency is calculated using the stream-tube model in order to iteratively identify an appropriate rotational speed for the turbine for a given blade length. Fig. 3 shows the variation of rated power with rotational speed for a rotor diameter of 24 m. In this case, peak power is developed at approximately 12 r.p.m, with the target of 1500 kW occurring somewhat lower. Fig. 3 also shows the relationship between hydrodynamic efficiency and rotational speed for a similar size rotor, where hydrodynamic efficiency is taken as being the percentage of the max power that can be extracted as defined by Betz Limit. Peak efficiency is seen to occur between 8 r.p.m. and 11 r.p.m. for this design.

An additional concern, relating to the rotor size and rotational speed, is cavitation inception along the blade. Cavitation has a number of detrimental effects on tidal turbine blades including accelerated wear of blade materials and increased load uncertainty along the blade [18]. Thus the avoidance of cavitation is a crucial design constraint, which is not taken into account by the BEMT and conventional stream-tube models. A cavitation check is incorporated into the stream-tube model. Cavitation can be predicted for tidal turbine blades by comparing the local pressure distribution with a parameter known as the cavitation number [19], σ, which is defined as follows [20]

$$\sigma = \frac{P_{AT} + \rho g h - P_V}{0.5 \rho V^2} \tag{10}$$

where P_{AT} is the atmospheric pressure which is taken as 101.3 kPa, P_V is the vapour pressure of seawater which is taken as 2 kPa, h is the head, which is the shortest distance between a passing blade tip and the free surface, and V is the local inflow velocity [12].

Step 5 – Cavitation check

With knowledge of the local inflow velocity at each point in the blade from the stream-tube model, the minimum cavitation number of the turbine blade as a whole can be found. Cavitation inception can then be checked by comparing the cavitation number at each blade section with the minimum negative coefficient of pressure of the hydrofoil [14]. If the local cavitation number drops below the pressure coefficient, cavitation will occur at the blade section. After testing various rotational speeds and blade lengths in the stream-tube model, a 12 m blade rotating at 10 r.p.m. was found,

for the present design, to be the longest blade length and highest rotational speed at which cavitation inception at the blade tip could be avoided. Fig. 4 plots the cavitation number against distance from the blade root for the chosen rotor dimensions and rotational speed.

The input parameters for the stream-tube model are summarised in Table 1.

2.2 Structural Model

2.2.1 Structural Design Process

A flowchart of the preliminary structural design process is shown in Fig. 5. This is described by the following algorithm:

Step 1 – Calculation of main blade loadings

The structural design begins with output from the hydrodynamic design process, in the form of the optimised turbine blade shape and size and the blade loadings. By treating the blade as a technical cantilever beam and with the thrust and tangential forces at each blade station output from the stream-tube model, the flapwise and edgewise bending moment distributions for the turbine blade are calculated.

Step 2 – Material selection

The bending moment distributions, in conjunction with the turbine operating environment and production costs, form the basis for material selection. The high bending moments predicted during operation require materials with high specific strength and stiffness in order for the blade to retain its shape under high loadings. Being immersed in corrosive seawater can lead to degradation of certain material properties over long periods of time. Therefore, the material used must resist this corrosive environment whilst still maintaining high levels of strength and stiffness. Also, as the blades are submerged in water depths of greater than 20 m, the likely maintenance windows are few and far between (due to the difficulty in accessing the blades from the surface). Hence, fibre- reinforced polymer composites, specifically GFRP and CFRP, which have been used extensively in the wind turbine industry, are the ideal construction material.

An appropriate composite layup, including a cross section thickness distribution, for the blade is then selected. Due to the non-uniform loading along the span of the blade, the thickness of the composite layup varies from the blade root to tip, with the root portion requiring significantly more material to offset the high bending moments it experiences. The maximum thickness at any given point along the blade is constrained by the chord length at that point, due to the dimensions of the blade profile being a function of the chord length distribution output from the stream-tube model. Using this maximum thickness as a starting point, an iterative design process, incorporating PreComp, is used to arrive at more streamlined thickness distribution.

Step 3 – Blade thickness distribution and composite lay-up selection

The PreComp program is used to compute relevant structural properties of the blade. Strain calculations for the blade spar caps are then carried out, using the aforementioned bending moment distributions and are detailed in section 2.2.2. This process involves refining the blade thickness distribution input into PreComp, based on the calculated maximum strains, where the strains are compared to the failure strain of the composite material, be it GFRP or CFRP. Beginning with the maximum allowable thickness, the amount of material is iteratively reduced until the maximum strain drops below the failure strain. When the failure strain is significantly exceeded and blade thickness is already at a maximum, a review of the material selection is required. A quasi-isotropic composite layup was used for most areas of the blade, owing to the multi-axial loading predicted during operation. Further details of the lay-up used for this present design are given in section 2.2.2

Step 4 – Strain concentration reduction

The presence of strain concentrations is dealt with by altering the thickness distribution near locations where ply drop-offs are expected, with a smooth and gradual reduction in thickness being preferable to a sudden drop.

Step 5 – Finite element analysis

With a preliminary lay-up decided upon using PreComp, a detailed finite element model is developed to provide a more accurate strain analysis. These results can be compared to the PreComp results. This detailed finite element model allows detailed

design for mitigation of strain concentrations along the blade through redesign of the internal blade structure. This also incorporates multi-axial loading effects which the PreComp analysis was unable to predict.

2.2.2 PreComp

Pre-Processor for Computing Composite Blade Properties, or PreComp as it is commonly known, is an open source code developed by *The National Wind Technology Center* [9] for use in computing various structural properties along the span of a wind turbine blade. Although envisaged for use in the wind energy sector, the code readily lends itself to the analysis of a tidal turbine blade with little modifications needed to the program code. The program outputs useful structural properties such as: flap-wise and edge-wise section stiffness, the mass of the blade per unit length and the section torsional stiffness amongst others. Knowing the blade stiffness and using the flapwise and edgewise bending moment distributions for the blade calculated from the hydrodynamic model, it is possible to estimate peak strains in the blade under typical operating conditions. The incentive to use PreComp is that it allows the designer of a turbine blade to rapidly alter the lay-up of the blade and evaluate the resulting effects on the structural integrity of the design. Thus, before beginning a detailed and costly finite element model analysis, it is possible to develop a coherent and efficient lay-up for the blade and to predict various blade structural properties with reasonable accuracy.

PreComp computes the stiffness and inertial properties of a composite blade at discrete points along the blade in a span-wise direction, with a modified version of conventional 2D laminate plate theory combined with a shear flow approach being relied on to calculate the section properties. A number of underlying assumptions are made by PreComp including:

- Each blade section is a thin-walled, closed section
- There are no hoop stresses in any wall of a section
- The blade is straight and has no built-in curvature
- Transverse shear is neglected
- Each blade section is free to warp out of its plane

For PreComp to compute a useful set of properties it requires the external hydrofoil shape and internal lamina layup of the blade. The main parameters for defining the external shape were obtained from the stream-tube model. From this model the variation in chord and twist of the blade could be calculated and used as input to PreComp. PreComp permits the use of multiple hydrofoil profiles along the length of the blade, with each profile being assigned a specific input file and radial position, and so is useful in determining the thickness variation of the outer blade profile which will lead to optimised hydrodynamic and structural performance. The internal structure is specified by the lamination schedule and the fibre orientation within each lamina. The code also allows for the placement of webs within the blade at user- specified locations.

PreComp does not define the internal structure of the blade as a single part, but rather splits the area up into a number of unique sectors, with each sector having its own composite lay-up. As seen in Fig. 6, the leading edge of the hydrofoil is named sector 1, the spar caps at the middle of the blade compose sector 2 and the trailing edge is defined by sector 3. In PreComp a sector is defined as a laminate, or stack of laminas composed of various materials. Each ply within this laminate is composed of a similar number of plies which are defined as input data. The hydrofoil profile is also divided into an upper surface and lower surface, each having three sectors. The number and position of the webs can also be chosen by the user. The material properties for blade coatings and composites are also given as input data.

PreComp is capable of dealing not only with the hydrofoil profile of the blade, but also with the circular root section which joins the blade to the turbine hub. Thus, the internal and external geometry of the blade can be specified in relative completeness. The material properties used for the structural model and input into PreComp are shown in Tables 2(a) and 2(b). Table 2(a) uses unidirectional (UD) GFRP for the spar caps while Table 2(b) has UD CFRP for the spar caps. The basic composite lay-up used for the PreComp calculations is shown in Table 3.

Although PreComp does not solve directly for the lamina strains, it does provide the user with enough information to make such calculations straightforward, provided one has access to the bending moment distribution along the blade. Using the section flapwise and edgewise stiffness calculated by PreComp it is possible to calculate the maximum strain at each blade section in a number of directions, as follows:

$$\varepsilon_{upper} = \frac{M_{flap} c_{upper}}{EI_{flap}} \tag{11}$$

$$\varepsilon_{lower} = \frac{M_{flap} c_{lower}}{EI_{flap}} \tag{12}$$

$$\varepsilon_{LE} = \frac{M_{edge} c_{LE}}{EI_{edge}} \tag{13}$$

$$\varepsilon_{TE} = \frac{M_{edge} c_{TE}}{EI_{edge}} \tag{14}$$

where ε_{upper} is the maximum strain above the chord line, M_{flap} is the flapwise bending moment at the blade station, c_{upper} is the distance between shear centre and upper most point on the hydrofoil profile, EI_{flap} is the flapwise bending stiffness at the blade station, ε_{lower} is the maximum strain below the chord line, c_{lower} is the distance between shear centre and lower most point on the hydrofoil profile, ε_{LE} is the strain at the leading edge of the blade, M_{edge} is the edgewise bending moment at the blade station, c_{LE} is the distance between the shear centre and leading edge of the hydrofoil, EI_{edge} is the edgewise bending stiffness at the blade station, ε_{TE} is the strain at the trailing edge of the blade and c_{TE} is the distance between the shear centre and trailing edge of the hydrofoil.

It should be noted that PreComp calculates the stiffness of the blade as a whole, treating the blade as an equivalent beam. This means lumping the stiffnesses of various sectors, which are defined in Fig. 6, together to produce an overall stiffness value for the blade. The spar caps, being the stiffest components, will therefore provide most of the blade's flexural stiffness. However, this has the effect of underestimating the maximum strain present in the spar caps. While this is not a major issue for a high modulus material such as CFRP, the strains given for GFRP should be regarded as the lowest possible value of strain that could be expected during operation as the relative contribution of the spar caps to the overall stiffness of the blade will be far less.

2.2.3 Finite Element Model

The finite element model of the blade represents the final design stage of the turbine blade using CFRP as the spar cap material and integrates the blade profile and loadings determined from the stream- tube model with the internal lay-up provided by PreComp. The finite element model offers a more detailed structural analysis of the blade than PreComp, but with significantly increased computational cost, of the order of 10^3 – 10^4 seconds compared to less than 10 seconds for PreComp. Unlike PreComp, the finite element model does not treat the blade as an equivalent beam as described in section 2.2.1, giving a more accurate prediction of the strain present in the spar caps. However the time required to create a 3D shell model of the blade and run the analysis means that PreComp remains an attractive analysis tool for initial design iterations. The first stage in the finite element analysis involved using *Inventor*, a parametric modelling tool, to create a 3D shell model of the blade. This model incorporates the chord and twist distributions determined from the stream-tube program as well as using three aerofoils from the *Riso A1* family (A1-24, A1-21, A1-18) to define the thickness distribution of the blade. This 3D model was then imported into the *Abaqus 6.9* finite element program, where the necessary loads and boundary conditions were applied to the blade as shown in Fig. 7. The composite lay-up used in PreComp was then added to the model.

The blade was modelled using 4-Node reduced integration (S4R) linear shell elements with enhanced hour-glass control. Under the plane stress conditions assumed by the shell elements, only the values of the longitudinal modulus E_1, transvers modulus E_2, major Poisson's ratio ν_{12} and shear modulii are required to define the orthotropic nature of the lamina. The stress strain relations for the in-plane components of the stress and strain are given as follows:

$$\begin{Bmatrix} \varepsilon_1 \\ \varepsilon_2 \\ \gamma_{12} \end{Bmatrix} = \begin{bmatrix} 1/E_1 & -\nu_{12}/E_1 & 0 \\ -\nu_{12}/E_1 & 1/E_2 & 0 \\ 0 & 0 & 1/G_{12} \end{bmatrix} \begin{Bmatrix} \sigma_{11} \\ \sigma_{22} \\ \tau_{12} \end{Bmatrix} \quad (15)$$

where ε_1, ε_2, and γ_{12} are the longitudinal, transverse and shear strains respectively, G_{12} is the in-plane shear modulus and σ_{11}, σ_{22}, and τ_{12} are the longitudinal, transverse and shear stresses respectively.

The blade model includes the circular transition area from the steel hub to the blade for completeness, although the strain analysis only commences at a distance of 2 m from the hub and continues to the tip as the hub area is beyond the scope of this work. A box spar configuration has been used to form the structural core of the blade and consists of two shear webs which run for a length of 7 m starting at the end of the transition area, at a 2 m radius from the centre. The spar caps, which form the top and bottom of this box structure, taper from 108 mm thick at a radius of 2 m to 45 mm thick at the blade tip.

The two main sources of loading on the blade, the thrust and tangential forces, were applied to the model as surface traction distributions. The surface tractions were applied directly to the spar caps of the blade, which is based on the assumption that the resultant loads acting on the blade act at a point which is 25% of the chord length back from the leading edge of the blade [10], with the spar cap sector of the structure starting at 15% of the chord length.

3. Results

3.1 Hydrodynamic Model Results

The chord length and twist angle distributions for the blade predicted by the stream-tube model described by the parameters in Table 1 are shown in Fig. 8 and Fig. 9 respectively. These distributions represent the chord length and twist angle calculated for each of the 45 stream-tubes into which the 12 m blade is divided. The chord length is largest near the root of the blade where it tapers from a maximum value of 1.625 m down to 0.658 m at the blade tip. The large chord length near the root of the blade is favourable for resisting the large bending moments that the blade will experience during operation, while the smaller chord found beyond mid-span will result in a thinner hydrofoil profile which will reduce drag and improve hydrodynamic performance [13]. The twist angle of the blade varies from 20° at the 2 m mark to 0.1° at the blade tip. A twist is built into the blade geometry for the same reason as for wind turbines where the apparent wind angle varies along the blade due to changing local speed ratio [21]. The blade needs to be turned in order to accelerate the fluid evenly across

the length of the blade for a given constant fluid flow. The apparent fluid flow increases in strength and its position moves towards the plane of rotation with increasing radius, outwards along the blade. In order to maintain an angle of attack of 6° while the blade speed is increasing, the angle of attack must decrease toward the tip [22].

The axial (thrust) and tangential force distributions calculated by the stream-tube model are shown in Fig. 10. The axial force is seen to increase linearly with radial distance along the blade from approximately 2.8 kN to 16.6 kN at the blade tip. The tangential force increases asymptotically with radius from 1.4 kN near the root to about 1.9 kN at the tip. The thrust force makes up one component of the fluid forces on the blade and it acts perpendicular to the hydrofoil chord line. The tangential force is what causes the power producing torque and acts parallel to the hydrofoil chord line [23]. The thrust force is noticeably larger than the tangential force resulting in a flapwise bending moment in excess of 3 MNm at the blade root compared with an edgewise moment of 0.5 MNm at the same position as shown in Fig. 11. The total torque produced by the turbine is 1.56 MNm which is found by multiplying each radial force component by its respective lever arm, which is its distance from the blade root, and summing the resulting moments over each of the three blades.

The tidal stream velocity at which the turbine is designed to produce its rated power of 1.5 MW is 2.4 ms^{-1}. The variation of root flapwise bending moment with tidal stream velocity is shown in Fig. 12. The bending moment increases four-fold for a doubling of velocity from 2 - 4 ms^{-1} highlighting the challenges tidal turbine designers face at modest fluid flow increases. Fig. 13 shows the variation of root flapwise bending moment with blade length for a constant tidal stream velocity of 2.4 ms^{-1}, with a doubling in blade length predicted to give a factor of 5 increase in maximum bending moment. The price of increasing blade length is a significant increase in root bending moment which may prove challenging if the tidal energy industry is to aim for the level of up-scaling achieved in the wind turbine industry.

3.2 PreComp Analysis Results

The blade spar caps, being the main load bearing members, tend to be subjected to the highest strains and are therefore the main focus of this study. Due to the high bending moments calculated, the initial composite lay-ups used are quite thick at the root and taper towards the tip. The thickness variation of the spar caps is shown in Fig. 14. A number of ply drops are

present along the thickness of the blade. This is due to the finite number of input files that can be specified for each blade section along the blade length, meaning a continuous variation in thickness is not possible to implement. When defining the lay-up for the finite element model a power law approximation of the PreComp thicknesses was used to provide a smooth variation in thickness. Two load cases were defined for the structural analysis: a normal load case with a tidal stream velocity of 2.4 ms^{-1} and an extreme load case of 4.1 ms^{-1}. The extreme load case represents the maximum tidal velocity that the blade is likely to encounter during its life. *McCann et al* [11], through consultation with the tidal stream industry, recommend an extreme tidal velocity of 4.1 ms^{-1} for a site where a tidal turbine would typically be located. Using this tidal stream velocity, the maximum flapwise bending moment acting on the blade was found to be of the order of 8 MNm with the moment distribution following the same radial distribution as shown in Fig. 11.

The maximum strains at each blade section are calculated using equations (10) - (13) using the stiffnesses predicted from PreComp and the bending moment distributions predicted by the stream-tube model. The flapwise strains in the spar caps are significantly larger than the edgewise strains due to the large thrust forces on the blade. Fig. 15(a) and (b) shows the predicted flapwise strain distribution for blades using GFRP and CFRP spar caps for extreme and normal load cases. The strains predicted by PreComp for the GFRP caps are far greater than the CFRP caps as expected. The maximum strain in the transition section (0.5 m - 2 m) has also been included and has a peak value of over 2.7 % for the GFRP under extreme load conditions, which as a ratio, is 0.98 of the tensile strain-to-failure of the *Advanced Composites Group's MTM28 Series* of high-performance unidirectional glass fibre epoxy laminates [24]. Even when using laminates with a thickness of over 100 mm, the strains obtained are too close to the failure strain of the material and with the majority of the blade experiencing 1% strain, the risk of failure over the lifetime of the turbine is significant. Tidal velocities of up to 4 ms^{-1} could conceivably occur numerous times over the lifespan of such a device.

Furthermore, the effect of sea water degradation of the fibre-matrix interface is likely to reduce the stiffness of the GFRP over time [25]. However, it is reasonable to assume that the maximum strain experienced by the blade should be significantly lower that the composite's ultimate strain due to the difficulties in replicating the complex multi-axial loads the blade is likely to experience when in operation [10]. The use of CFRP for the spar caps is shown to

greatly improve the stiffness of the blade, with the maximum strain registered being approximately 4 times lower than for GFRP for a similar lay- up. A factor of safety greater than 2 is obtained for the extreme load case, with 75% of the blade registering a strain 5 times below the maximum allowable of 1.5% for the material properties used [26].

Although a detailed fatigue life analysis was not carried out in this study, preliminary calculations suggested that up to a 50% knock-down in static failure strain could be expected for the spar caps over a 20 year life span, which translates into 10^7 cycles of reversed loading. With this in mind, it is likely that fatigue loading will be the critical design criterion [10]. It should be noted that PreComp has a tendency to underestimate the maximum strains and a considerable factor of safety is required to account for possible degradation of the composite when exposed to seawater. The specific stiffness of the CFRP is clearly far superior to the GFRP material. However, this increase in stiffness comes at a price, with CFRP material being typically 7-8 times more expensive than GFRP material [21]. For this reason, use of the carbon fibre composite is restricted to the spar caps of the blade. An added benefit of using CFRP is that it reduces the overall weight of the blade by about 13% as predicted by PreComp. Table 4 summarises the main results from the PreComp analysis.

3.3 Finite Element Results

A comparison between the maximum flapwise strain distribution as calculated by PreComp and the finite element model is shown in Fig. 16. Good agreement between the models is observed, with PreComp underestimating the strain values by about 16% for maximum strain (blade root) and by approximately 30% at a 5 m radius from the root. This can partly be attributed to the method by which PreComp calculates the stiffness of the blade which involves lumping all the sectors together to form an equivalent beam, while the finite element model is able to model accurately the geometric complexity of the airfoil section. This highlights the use of PreComp as a precursor to the costly finite element analysis, with key blade structural properties being estimated with good accuracy. Note that the discontinuities in the strain distributions can be attributed to ply drops in the case of the PreComp model and due to changes in the hydrofoil profile in both models such as at the 10 m radius, where the hydrofoil switches from a Riso A1-24 to the more slender Riso A1-18. Fig. 17 shows the flapwise deflection of the blade under extreme load conditions, with the tip deflection of 1.75 m comparing quite well with the 1.76 m predicted by PreComp. The main results of the finite

element analysis are provided in Table 5. The maximum strain values in the CFRP spar caps were as expected, with a peak value of 0.8% for the upper spar caps. The maximum strain in the blade root was 0.9% under full load conditions at a max tidal stream velocity of 4.1 ms^{-1} which represents an extreme load scenario. With 1.5% strain being the max allowable for the CFRP, this represents a factor of safety of 1.6 under extreme conditions. Under normal operating conditions, the strain in the root falls to approximately 0.3%, giving a factor of safety of 5 for the static design. Due to the difficulties in predicting the fatigue performance of composites immersed in seawater and a predicted lifespan of 10^7 cycles over 20 years such a large factor of safety is justifiable for initial designs [20].

3.4 Key Results and Discussion

The main results of this study are:

• Axial (thrust) forces represent the most significant loading on tidal turbine blades, with the resulting flapwise bending moment being 6 times larger than the edgewise moment for a 12 m blade in a 2.4 ms-1 tidal stream.

• Extremely high bending moments may prohibit up-scaling of designs to the extent seen in the wind turbine industry, with a 50% increase in the blade length of 12 m resulting in a three-fold increase in the flapwise bending moment at the blade root. This would entail significant additional structural reinforcement with the blade's spar caps comprising the majority of the overall blade thickness – even with high performance CFRP.

• The design code PreComp was used to determine the blade's structural properties which were then used to calculate the strain distribution along the blade for both GFRP and CFRP blades. It was discovered that for a commercial scale tidal turbine (1.5 MW) with 12 m blades, the bending moments predicted by the stream-tube model at normal and extreme loads resulted in significant strains in GFRP that would result in fibre failure. CFRP offered a noticeable improvement in the maximum strain levels, being well below the tensile failure strain of the material used in the models. It is reasonable to conclude from the above results that GFRP is not a suitable material to use to construct the main structural components of a large tidal turbine blade.

• Finite element results for the blade were compared with the PreComp results for the CFRP blade. Good agreement was observed between the models, with the finite element model predicting slightly higher strain values in general. A factor of safety of 1.6 was predicted for the CFRP blade under extreme load conditions.

• The calculated thickness of the spar caps (up to 108 mm near the root of the blade with a total blade weight of 1950 kg) would require a significant quantity of CFRP for construction with significant implications for production costs as compared to GFRP blades.

• It is likely that due to the 10^7 cycles of reversed loading that a tidal turbine will experience over a 20 year lifespan and the degradation of composites exposed to sea-water that fatigue loading will be the critical design criterion for the blade.

4. Conclusions

A combined hydrodynamic-structural design methodology for a commercial scale tidal turbine has been presented. A hydrodynamic analysis of the blade was carried out using BEMT to determine force distributions along the blade span under normal and extreme operating conditions as well as to create an optimised blade shape. Output from this model was used in a pre-processor for computing blade structural properties (PreComp) to determine the strain distribution along the blade spar caps. The strain distributions from this analysis were then compared with a more detailed and realistic finite element model of the blade, which is then used to compare the structural performance of GFRP and CFRP as spar cap materials.

A number of conclusions can be drawn from this study. The hydrodynamic analysis highlighted the significant loadings acting on tidal turbine blades, even at modest flow velocities. Large flapwise bending moments, in particular, are likely to be a major constraint on up-scaling of turbine designs. High bending moments under normal and extreme operating conditions were predicted to induce significant strains in GFRP spar caps, up to the point of fibre failure. Maximum strain levels in CFRP spar caps under similar loading conditions were found to be substantially reduced and well below the failure strain of the material. Using CFRP, the maximum spar cap thickness is estimated at over 100 mm for a 12 m blade, indicating that high manufacturing costs are likely.

The effectiveness of PreComp as a structural analysis tool for use in early design iterations has been established through the calculation of maximum strains accurate to within 16% of detailed three-dimensional finite element predictions, at critical locations such as the blade root, but, crucially, at a fraction of the computational cost.

Future work will involve experimental testing of tidal turbine blades for static strength characterisation. This testing is envisaged to focus on small-scale models of turbine blades with subsequent validation against full-sized blades. One of the key challenges associated with this proposed experimental work is the development of a large-scale test facility.

Fatigue strength prediction and comprehensive fatigue testing for both small-scale and full-sized turbine blades will also be required. The result of this work will help in incorporating the combined effects of sea water ingress and multi-axial cyclic stress/strain conditions on the fatigue life of the GFRP/CFRP into the existing design methodology.

Multi-scale finite element modelling of the damage progression in polymer composites used in tidal turbine blades (and ocean and wind energy applications in general) will underpin future blade designs. These models will likely range from examining crack initiation in multi-phase micro-scale unit cells to inter/intra-lamina delamination exacerbated by complex multi-axial loading and material property degradation due to immersion in sea water.

5. References

[1] Watchorn M., Trapp T. & Sayigh A.A.M. (2000). Tidal Stream Renewable Offshore Power Generation. *World Renewable Energy Congress* VI. Oxford Pergamon, pp.2664-2667.

[2] Hwang I.S., Lee Y.H. & Kim S.J. (2009). Optimization of cycloidal water turbine and the performance improvement by individual blade control. *Applied Energy*, vol. 86, pp. 1532-1540.

[3] O'Rourke F., Boyle F. & Reynolds A. (2010). Marine current energy devices: Current status and possible future applications in Ireland. *Renewable and Sustainable Energy Reviews*, vol. 14(3), pp. 1026-1036.

[4] Batten W.M.J., Bahaj A.S., Molland A.F. & Chaplin J.R. (2006). Hydrodynamics of marine current turbines. *Renewable Energy*, vol. 31, pp. 249-256.

[5] Nicholls-Lee R. F., Turnock S. R. & Boyd, S. W. (2008). Simulation based optimisation of marine current turbine blades. *7th International Conference on Computer and IT Applications in the Maritime Industries (COMPIT'08), Liège, Belgium 21 - 23 Apr 2008*. Liège, Belgium, Architecture Navale, Génie Maritime, Navigation Intérieure et Maritime, Analyse des Systèmes de Transport, pp. 314-328.

[6] Brondsted P., Holmes J. & Sorensen B. (2008). Wind Rotor Blade Materials Technology. *European Sustainable Energy Review Issue 2*, Riso National Laboratory for Sustainable Energy, Denmark.

[7] Glauert H. (1926). The elements of airfoil and airscrew theory. Cambridge: Cambridge University Press.

[8] Charles D. (2009). Prediction of the Performance of a Contra-rotating Tidal Turbine. Thesis for Master of Science in Energy Systems and the Environment, University of Strathclyde.

[9] Bir G. (2008). NWTC Design Codes (PreComp by Gunjit Bir).
URL: http://wind.nrel.gov/designcodes/preprocessors/precomp/. Accessed 13/11/2012.

[10] Kennedy C.R., Leen S.B. & Ó Brádaigh C.M. (2012). A preliminary design methodology for fatigue life prediction of polymer composite for tidal turbine blades. *Journal of Materials Design and Applications*, vol. 226, pp. 203-218.

[11] McCann G., Thomson M. & Hitchcock S. (2008). Implications of Site-specific Conditions on the Prediction of Loading and Power Performance of a Tidal Stream Device. *2nd International Conference on Ocean Energy* (ICOE 2008), 15-17 October, 2008.

[12] Blunden L.S. & Bahaj A.S. (2006). Initial evaluation of tidal stream energy resources at Portland Bill, UK. *Renewable Energy*, vol. 31, pp. 121-132.

[13] Fuglsang P. & Bak C. (2004). Development of the Riso Wind Turbine Airfoils. *Wind Energy*, vol. 7, pp.145-162.

[14] Beertagnolio F., Sorensen N., Johansen J. & Fuglsang P. (2001). Wind Turbine Airfoil Catelogue. Riso National Laboratory, Roskilde, Denmark.

[15] K. McClure Morton, Queens University Belfast, Natural Power Consultants. (2004). Tidal and Current Energy Resources in Ireland. Sustainable Energy Authority of Ireland.

[16] Walkington I. & Burrows R. (2009). Modelling tidal stream power potential. *Applied Ocean Research*, vol. 31, pp. 239-245.

[17] The exploitation of tidal marine currents. (1996). Report EUR 16683EN, DG Science, Research and Development, The European Commission Office for Official Publications, Luxembourg.

[18] Pierson S. (2009). Composite Rotor Design for a Hydrokinetic Turbine. Honors Thesis Projects,University of Tennessee Honors Program.

[19] Carlton J.S. (1994). Marine propellers and propulsion. Butterworth, Heinemann.

[20] Betz A. (1920). Das Maximum der theoretisch möglichen Ausnützung des Windes durch Windmotoren. *Zeitschrift für das gesamte Turbinenwesen*, vol. 26, pp. 307–309.

[21] Wind Energy Composite Materials Handbook, Gurit.
URL: http://www.gurit.com/wind-energy-handbook.aspx. Accessed: 13/11/2012.

[22] Gipe P. (2004). Wind Power, Renewable Energy for Home, Farm, and Business. Sterling Hill.

[23] Hau E. (2006). Wind Turbines: Fundamentals, Technologies, Application, Economics. Springer.

[24] Advanced Composites Group's MTM28 Series GFRP.
URL: www.advanced-composites.co.uk. Accessed: 13/11/2012.

[25] Segovia F., Salvador M., Sahuquillo O. & Vincente A. (2007). Effects of Long-term Exposure on E-glass Composite Material Subjected to Stress Corrosion in a Saline Medium. *Journal of Composite Materials*, vol. 41, pp. 2119-2128.

[26] Hexcel's AS4/3501-6 Carbon/Epoxy unidirectional prepreg.
URL: www.hexcel.com. Accessed: 13/11/2012.

Tables

Table 1 Parameters for stream-tube mode under normal operating conditions

Parameter	Value
Number of Blades	3
Blade Length (m)	12
Tidal Current Velocity (ms^{-1})	2.4
Lift-to-drag Ratio	70
Lift Coefficient	1.15
Angle of Attack (Degrees)	6
Rate of Rotation (R.P.M.)	10
Density of Seawater (kgm^{-3})	1025
Kinematic Viscosity of Seawater (Pas)	0.0013155

Table 2(a) Material properties used in the structural model for the GFRP blade where UD is unidirectional and DB is double-bias. The material is *Advanced Composites Group's MTM28 Series* of high-performance unidirectional glass fibre epoxy laminates [24]

Material	E_1 (GPa)	E_2 (GPa)	G_{12} (GPa)	ν_{12}	Density (kgm^{-3})	Sectors
UD GFRP	38.8	10.0	2.7	0.28	1950	2, Webs
DB GFRP	22.0	22.0	2.7	0.30	1850	1,2,3
Gelcoat	1×10^{-8}	1×10^{-8}	1×10^{-9}	0.30	1830	1,2,3
Corecell	0.044	0.044	0.020	0.30	65	3, Webs

Table 2(b) Material properties used in the structural model for the CFRP blade. The CFRP used for the spar caps was *AS4/3501-6* Carbon/Epoxy unidirectional prepreg which is manufactured by *Hexcel* [26]

Material	E_1 (GPa)	E_2 (GPa)	G_{12} (GPa)	ν_{12}	Density (kgm^{-3})	Sectors
UD CFRP	142.0	10.3	7.2	0.27	1580	2, Webs
DB GFRP	22.0	22.0	2.7	0.30	1850	1,2,3
Gelcoat	1×10^{-8}	1×10^{-8}	1×10^{-9}	0.30	1830	1,2,3
Corecell	0.044	0.044	0.020	0.30	65	3, Webs

Table 3 Composite lay-up used in the structural model of the blade

Sector	Composite Lay-up
1	[45/-45/0/90/90/0/-45/45]
2	[45/-45/0/-45/45]
3	[45/-45/-45/45] Sandwich
Webs	[45/-45/-45/45] Sandwich

Table 4 Main results of the structural analysis using output from PreComp for the conditions outlined in Table 3

Material	Max. Strain-Extreme (%)	Max. Strain-Normal (%)	Tip Deflection-Extreme (m)	Tip Deflection-Normal (m)	Total Blade Weight (kg)
GFRP	2.72	0.91	4.10	1.36	2250
CFRP	0.73	0.24	1.76	0.60	1950

Table 5 Summary of main results from the finite element model of the CFRP under normal and extreme load conditions

Output Variable (Maximum Value)	Extreme Load	Normal Load
Strain in root	0.90%	0.30%
Flapwise strain in spar caps	0.80%	0.27%
Edgewise strain in leading edge	0.50%	0.17%
Shear strain in trailing edge	0.49%	0.16%
Flapwise deflection	1.75 m	0.58 m
Edgewise deflection	0.42 m	0.14 m

FIGURES

Figure 1 Vector diagram of velocities and forces for a blade element at a given radius.

Figure 2 Flowchart of the hydrodynamic modelling process.

Figure 3 Variation of rated power and hydrodynamic efficiency with rotational speed for a 12 m blade operating under a tidal stream velocity of 2.4 ms^{-1}.

Figure 4 Variation of Cavitation Number along the span of a 12 m blade rotating at 10 r.p.m.

Figure 5 Flowchart showing the structural modelling process.

Figure 6 Internal structure of the blade and sector definitions as used in PreComp, where sector 2 defines the spar caps of the blade.

Figure 7 Finite element model of 12 m tidal turbine blade showing the applied forces corresponding to a 2.4 m/s tidal stream velocity.

Figure 8 Chord length distribution calculated using the hydrodynamic model.

Figure 9 Twist angle distribution calculated using the hydrodynamic model.

Figure 10 Axial and tangential force distributions calculated using the hydrodynamic model for a tidal stream velocity of 2.4 m/s.

Figure 11 Flapwise and edgewise bending moment distribution calculated using output from the hydrodynamic model for a tidal stream velocity of 2.4 m/s.

Figure 12 Variation of max root flapwise bending moment with tidal stream velocity as predicted by the hydrodynamic model.

Figure 13 Variation of max root flapwise bending moment with blade length as predicted by the hydrodynamic model for a tidal stream velocity of 2.4 m/s.

Figure 14 Spar cap thickness distribution used in the PreComp model. A Power law approximation was used to input the thickness distribution into the finite element model.

Figure 15 Maximum flapwise strain in the blade's spar caps using GFRP and CFRP calculated using output from PreComp for tidal stream velocities of (a) 4.1 m/s and (b) 2.4 m/s.

Figure 16 Comparison of the max flapwise strain in the spar caps between the finite element model (FEA) and PreComp model of the CFRP blade for a tidal stream velocity of 4.1 m/s.

Figure 17 Flapwise deflection of the blade due to a tidal stream velocity of 4.1 m/s.

Appendix

Notation

a	axial flow induction factor
a'	tangential flow induction factor
C_D	aerofoil drag coefficient
C_L	aerofoil lift coefficient
c	chord length of the blade
c_{LE}	distance between the shear centre and leading edge of the hydrofoil
c_{TE}	distance between the shear centre and trailing edge of the hydrofoil
c_{lower}	distance between shear centre and lower most point on the hydrofoil profile
c_{upper}	distance between shear centre and upper most point on the hydrofoil profile
E_1	longitudinal modulus
E_2	transverse modulus
EI_{edge}	edgewise bending stiffness at the blade station
EI_{flap}	flapwise bending stiffness at the blade station
F_A	axial force component
F_t	tangential force component
G_{12}	in-plane shear modulus
M_{edge}	edgewise bending moment at the blade station
M_{flap}	flapwise bending moment at the blade station
N	number of blades on the turbine
r	radial location of the blade station
U_d	axial stream velocity at rotor disc
U_∞	free stream tidal velocity
W	resultant relative velocity the blade experiences
α	angle of attack
β	blade pitch angle
γ_{12}	in-plane shear strain
δD	magnitude of drag force at each span-wise location
δL	magnitude of lift force at each span-wise location
δr	length of blade station along span
ε_1	longitudinal strain
ε_2	transverse strain
ε_{LE}	strain at the leading edge of the blade
ε_{TE}	strain at the trailing edge of the blade
ε_{lower}	maximum strain below the chord line
ε_{upper}	maximum strain above the chord line
ν_{12}	major Poisson's ratio
ρ	density of fluid
σ_{11}	longitudinal stress
σ_{22}	transverse stress
τ_{12}	in-plane shear stress
v_b	tangential velocity of a blade element
v_t	the net tangential flow velocity of a blade element
φ	angle at which resultant velocity acts to the plane of rotation of the blade
ω	angular velocity of the blade

Abbreviations

GFRP	Glass fibre reinforced polymer
CFRP	Carbon fibre reinforced polymer
BEMT	Blade element momentum theory
PreComp	Pre-Processor for computing composite blade properties
UD	Unidirectional
DB	Double-bias
FEA	Finite element analysis

Figure 1

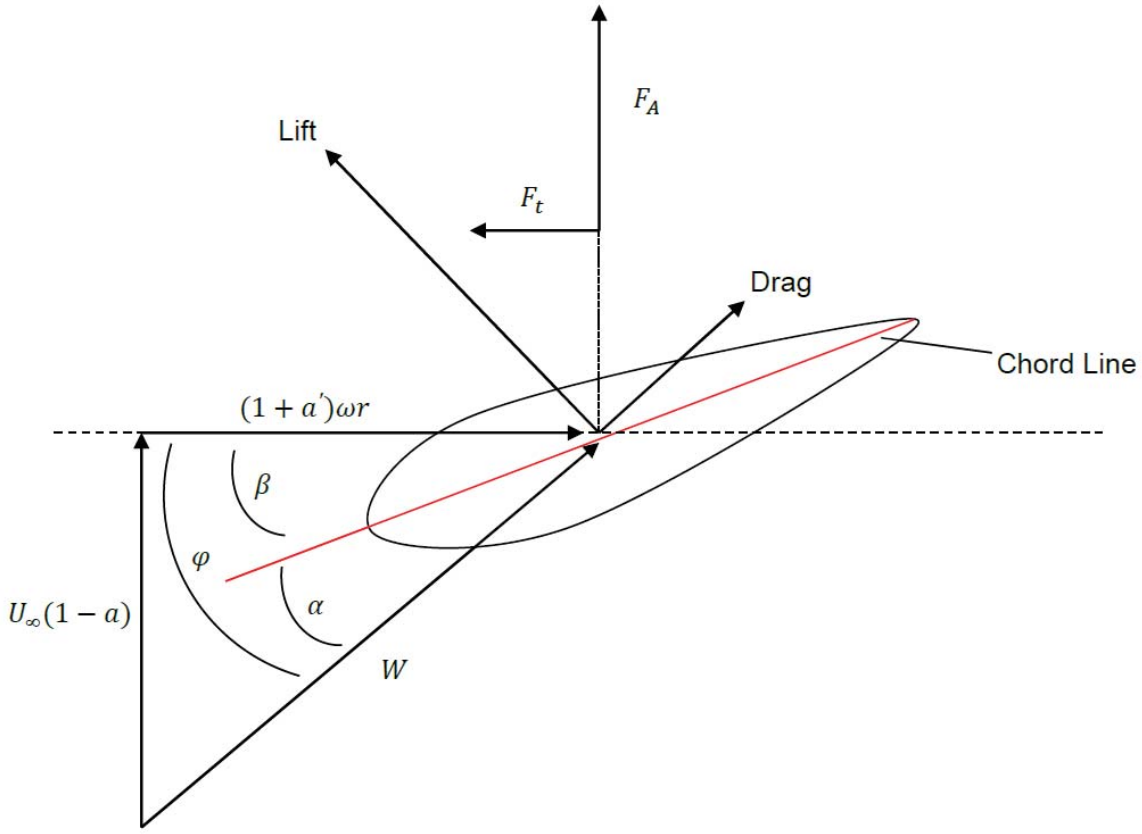

Vector diagram of velocities and forces for a blade element at a given radius

Figure 2

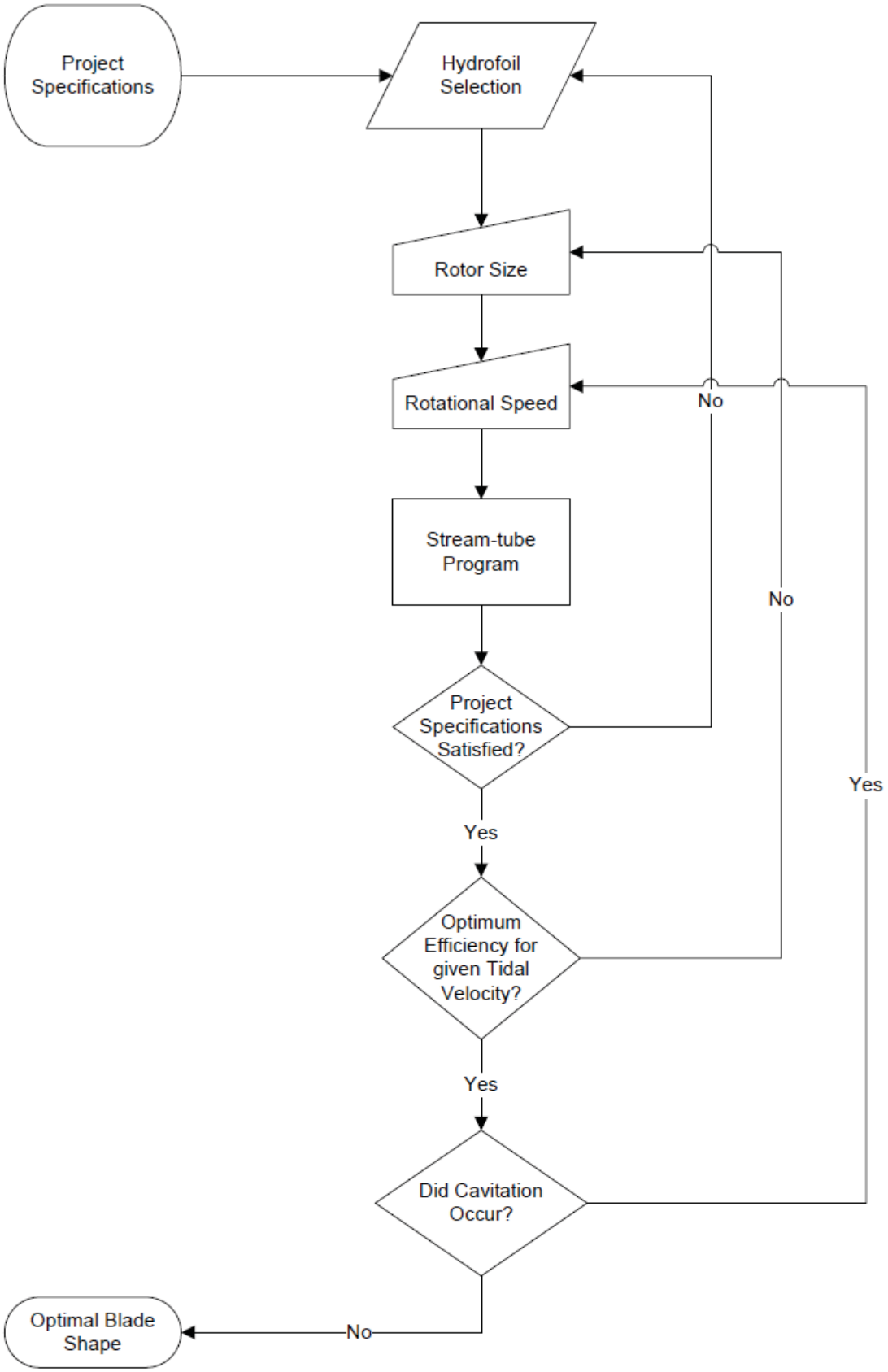

Flowchart of the hydrodynamic modelling process.

Figure 3

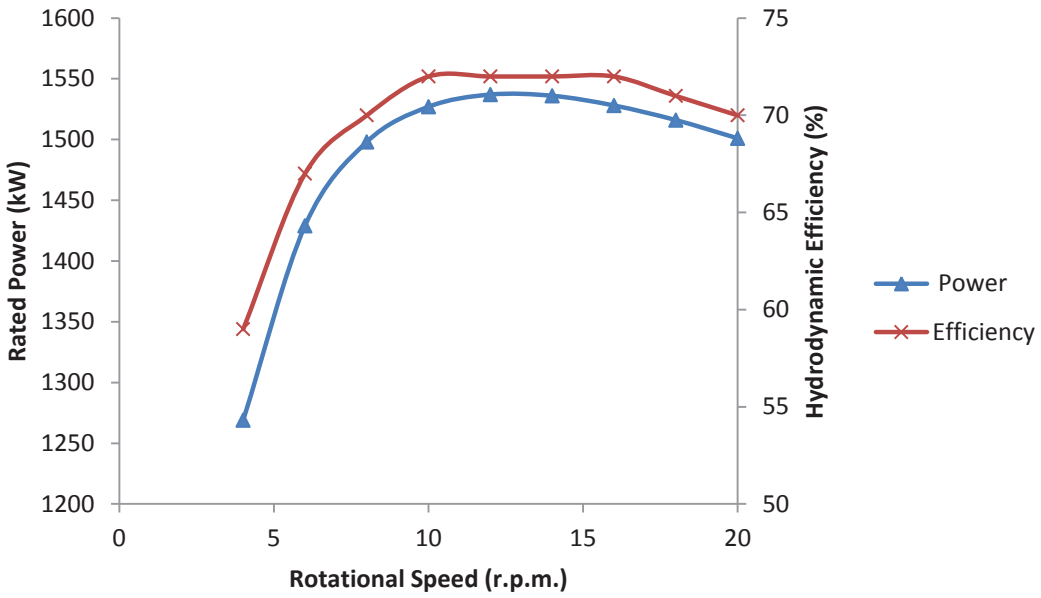

Variation of rated power and hydrodynamic efficiency with rotational speed for a 12 m blade operating under a tidal stream velocity of 2.4 ms^{-1}

Figure 4

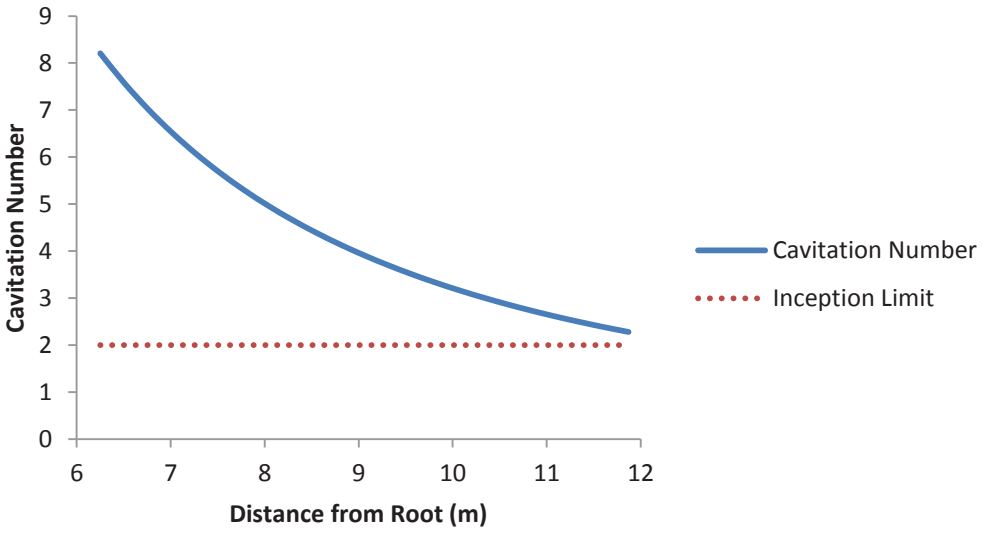

Variation of Cavitation Number along the span of a 12 m blade rotating at 10 r.p.m.

Figure 5

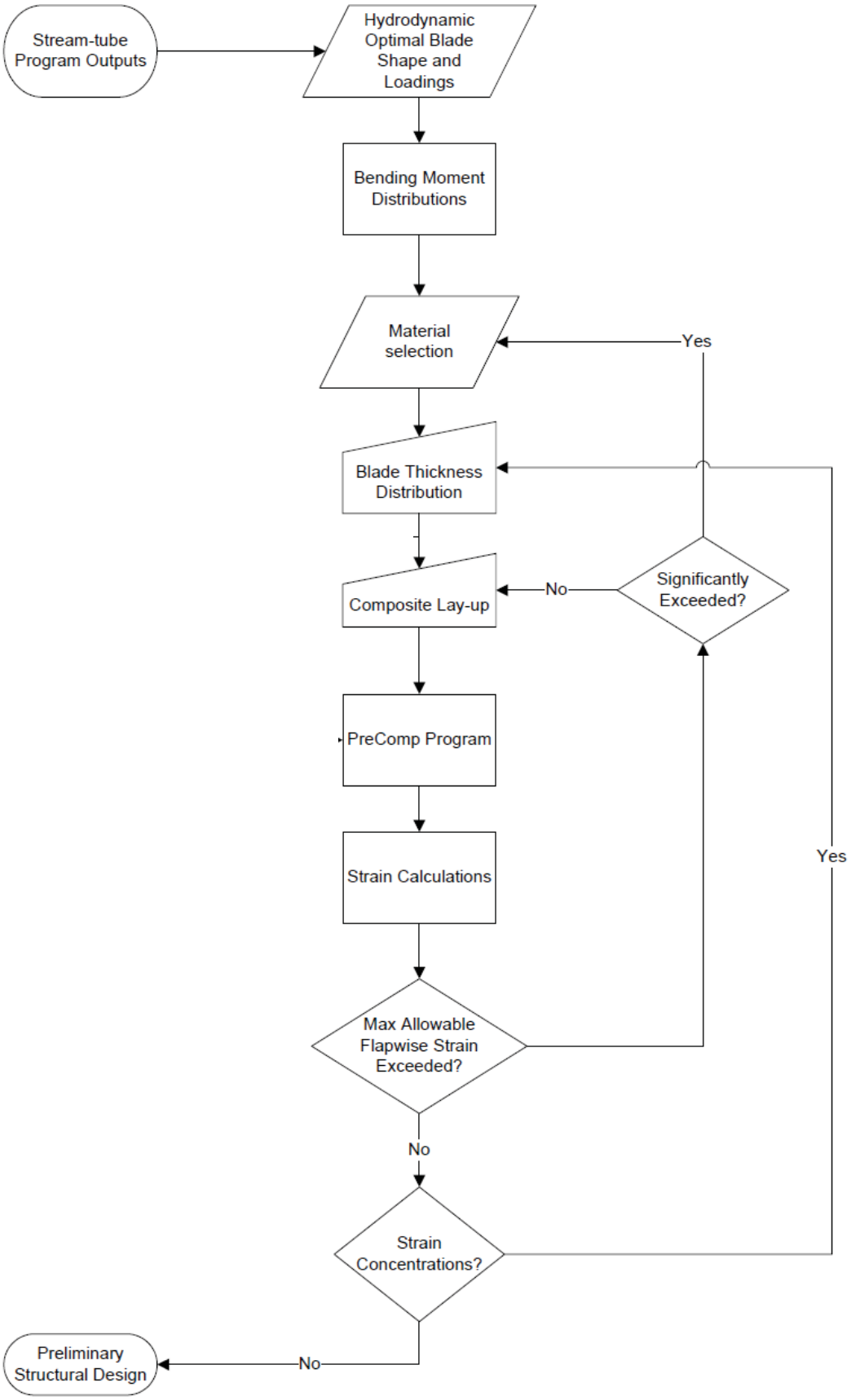

Flowchart showing the structural modelling process.

Figure 6

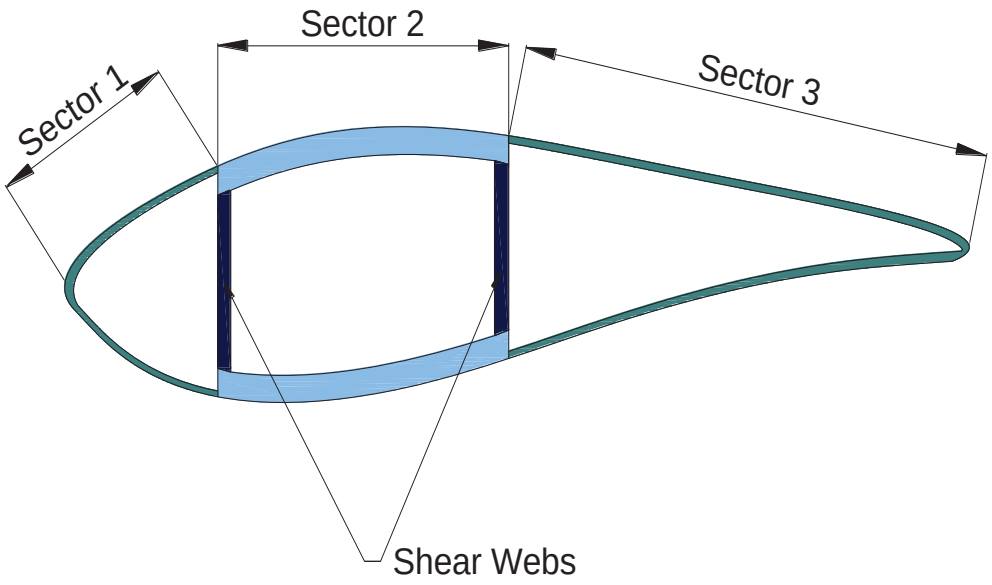

Internal structure of the blade and sector definitions as used in PreComp, where sector 2 defines the spar caps of the blade.

Figure 7

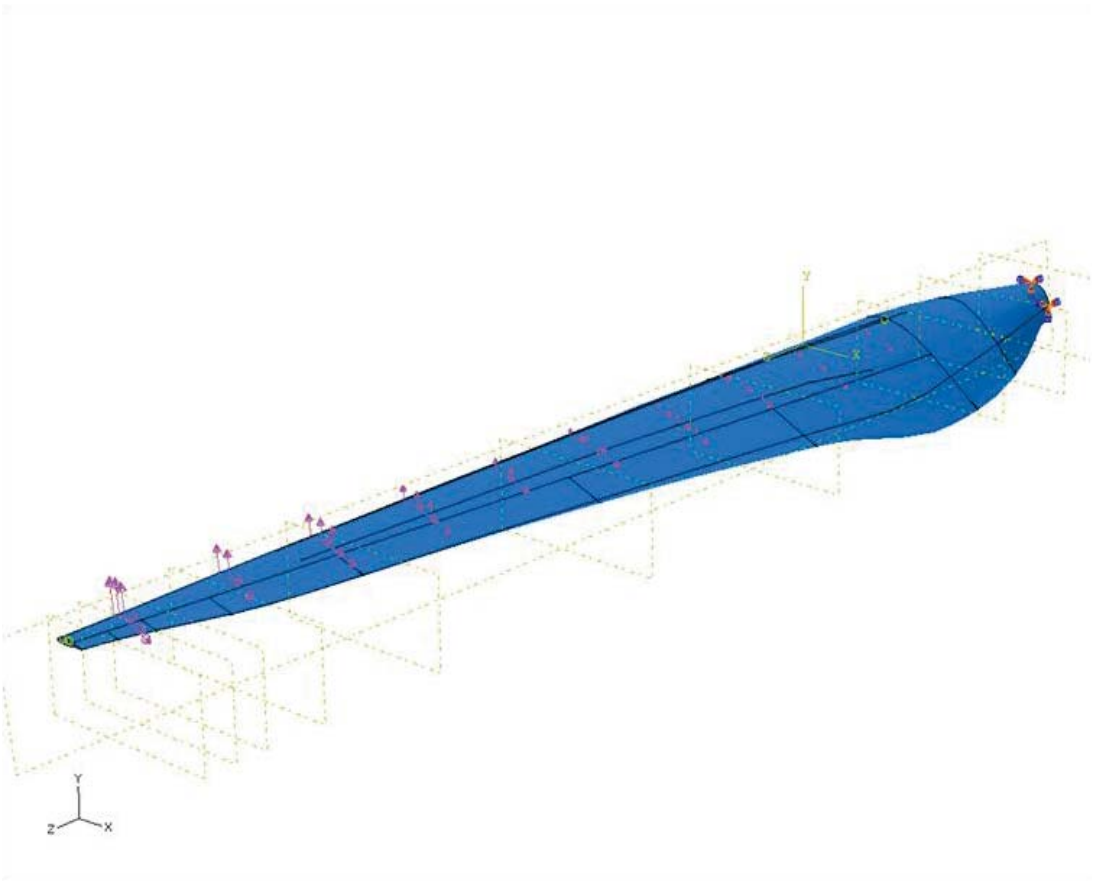

Finite element model of 12 m tidal turbine blade showing the applied forces corresponding to a 2.4 m/s tidal stream velocity.

Figure 8

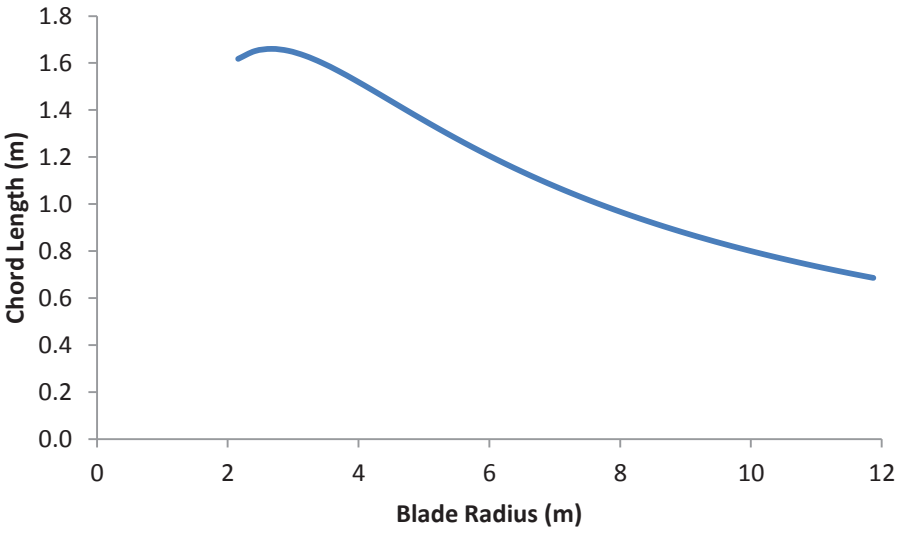

Chord length distribution calculated using the hydrodynamic model.

Figure 9

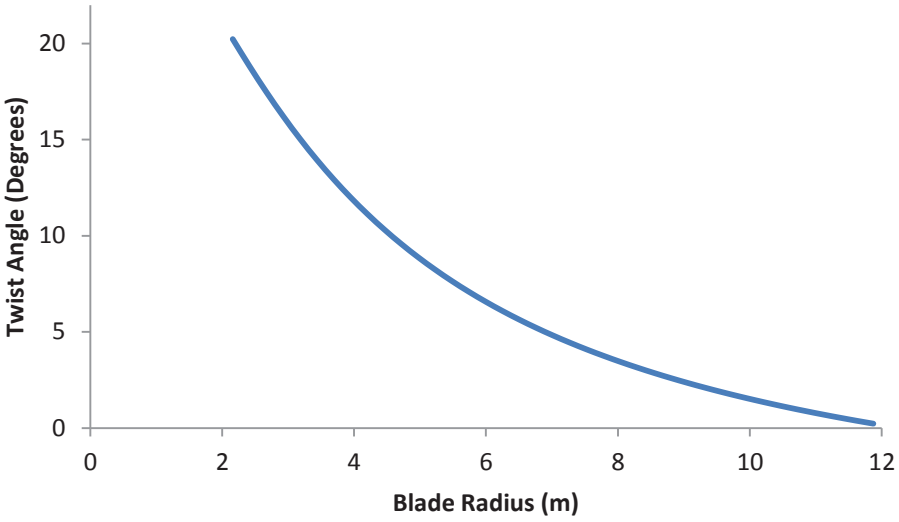

Twist angle distribution calculated using the hydrodynamic model.

Figure 10

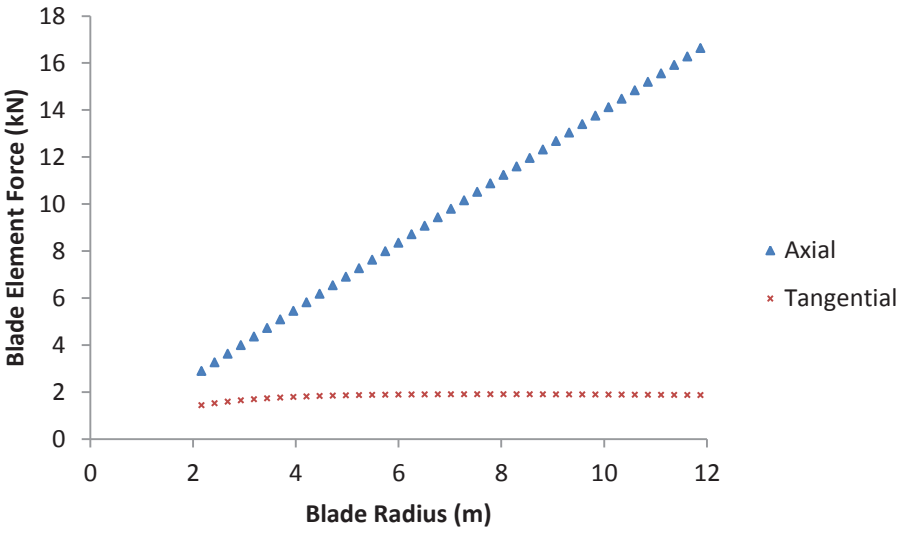

Axial and tangential force distributions calculated using the hydrodynamic model for a tidal stream velocity of 2.4 m/s.

Figure 11

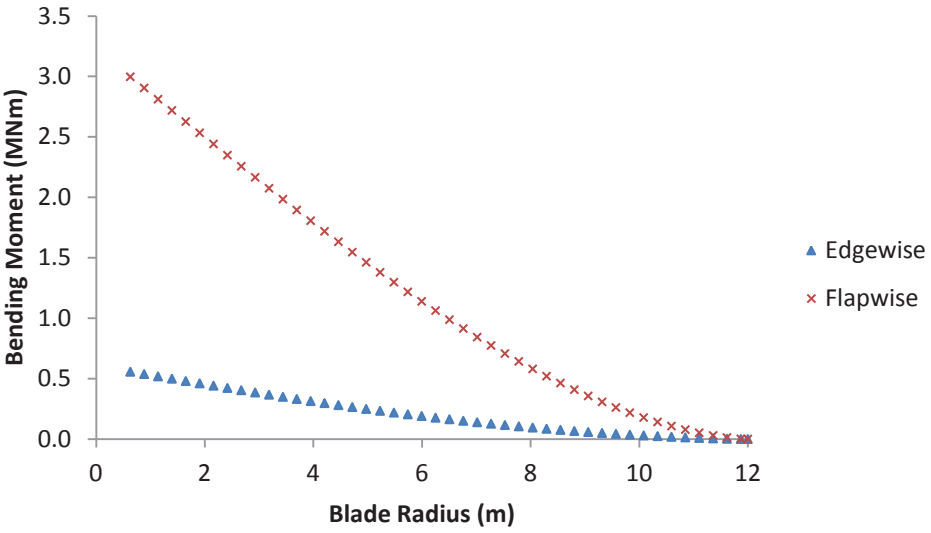

Flapwise and edgewise bending moment distribution calculated using output from the hydrodynamic model for a tidal stream velocity of 2.4 m/s.

Figure 12

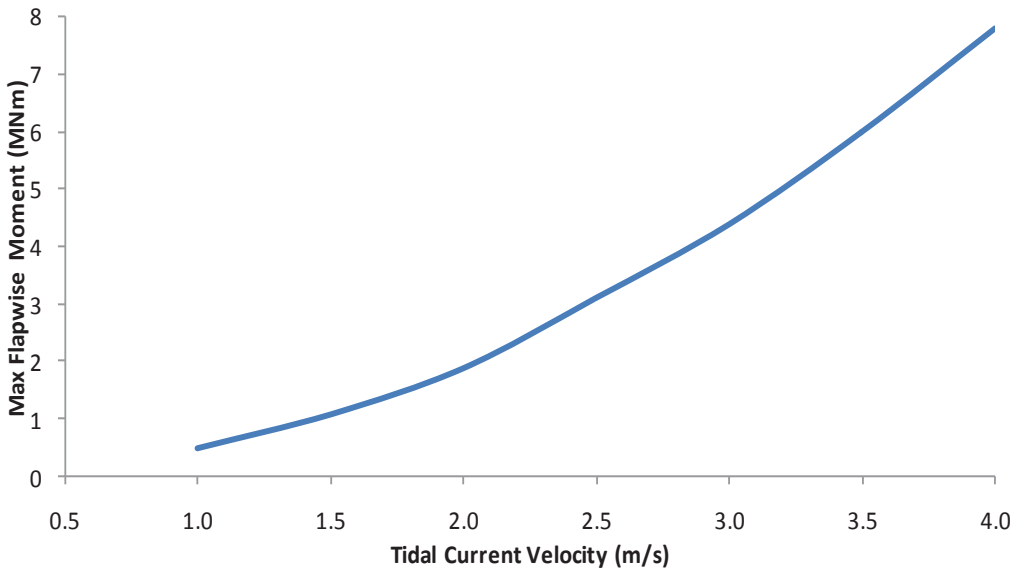

Variation of max root flapwise bending moment with tidal stream velocity as predicted by the hydrodynamic model.

Figure 13

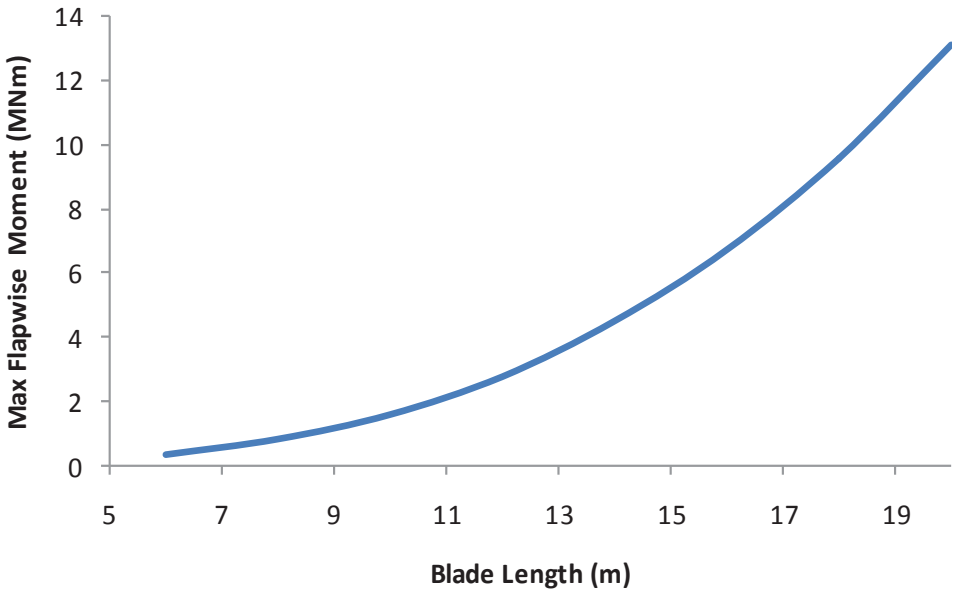

Variation of max root flapwise bending moment with blade length as predicted by the hydrodynamic model for a tidal stream velocity of 2.4 m/s.

Figure 14

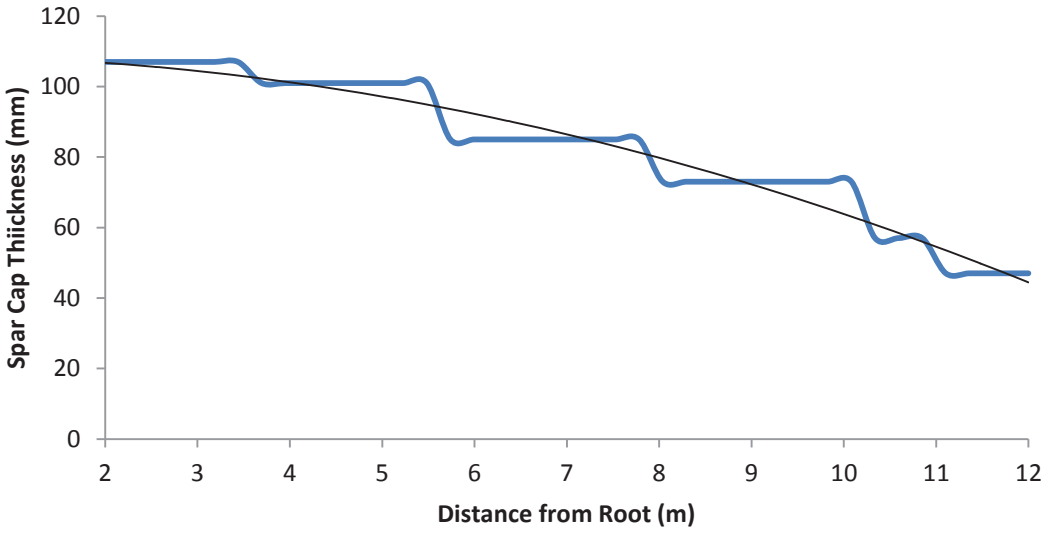

Spar cap thickness distribution used in the PreComp model. A Power law approximation was used to input the thickness distribution into the finite element model.

Figure 15

(a)

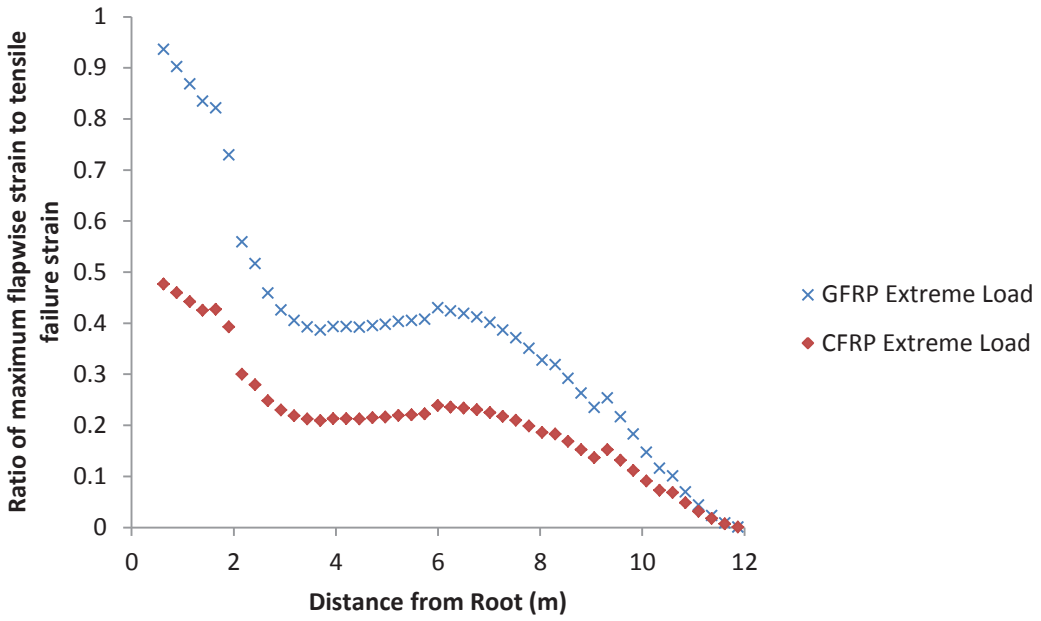

(b)

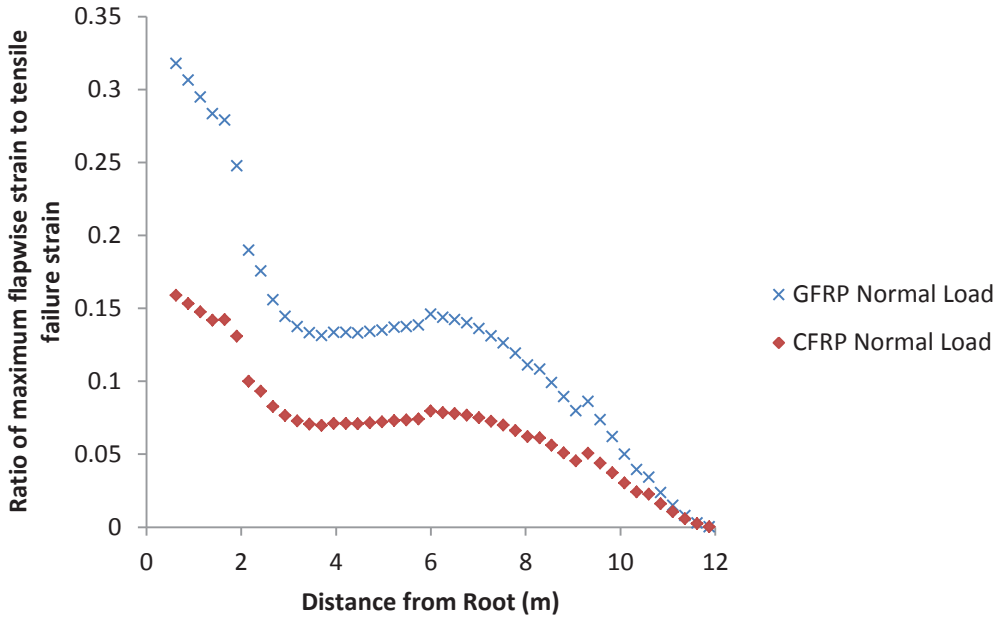

Maximum flapwise strain in the blade's spar caps using GFRP and CFRP calculated using output from PreComp for tidal stream velocities of (a) 4.1 m/s and (b) 2.4 m/s.

Figure 16

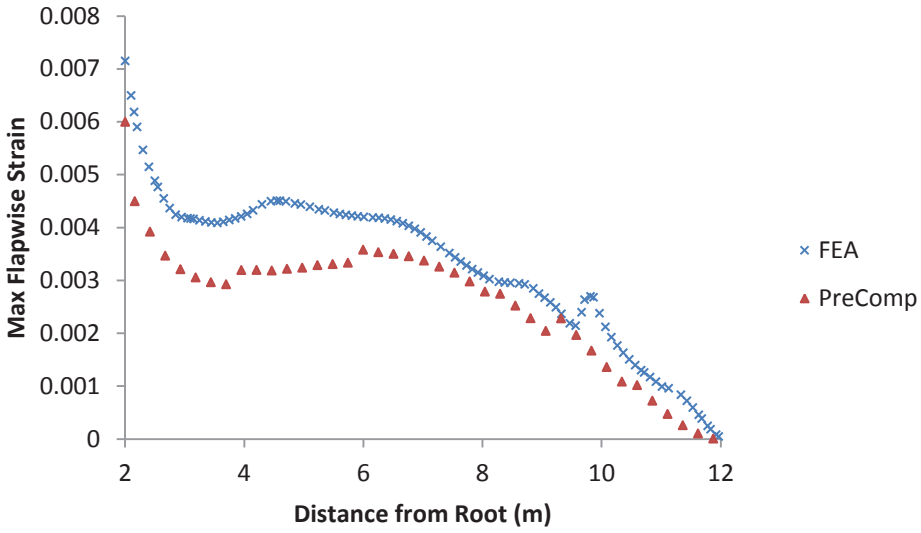

Comparison of the max flapwise strain in the spar caps between the finite element model (FEA) and PreComp model of the CFRP blade for a tidal stream velocity of 4.1 m/s.

Figure 17

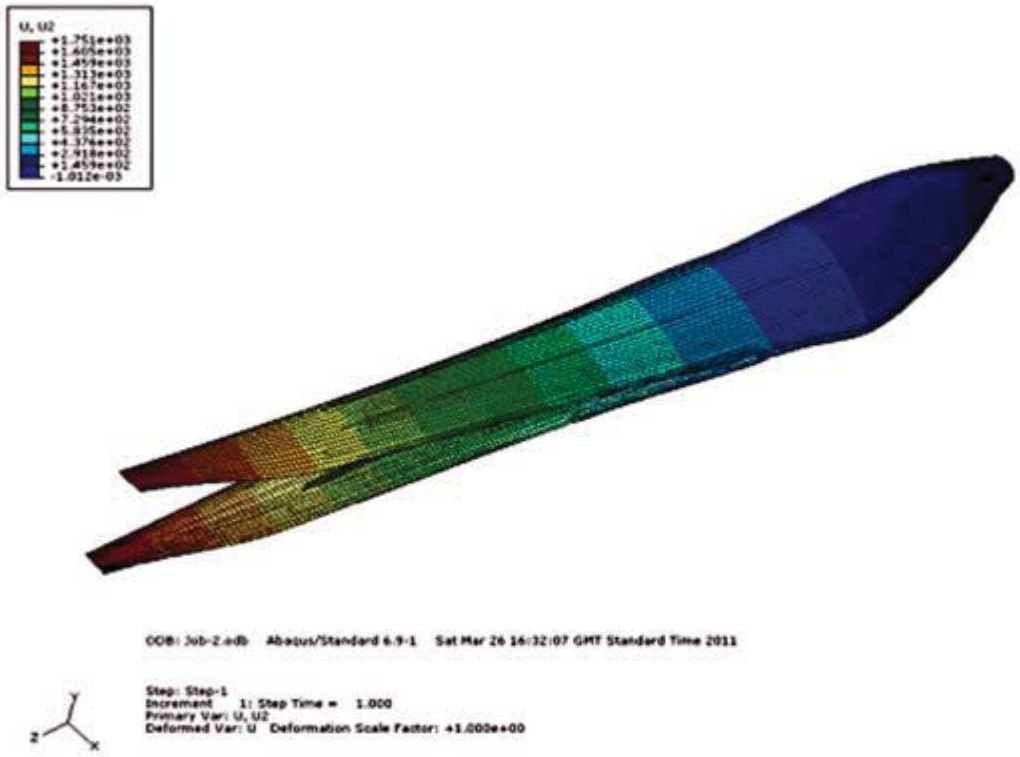

Flapwise deflection of the blade due to a tidal stream velocity of 4.1 m/s.